Cardiolipin and electron transport chain abnormalities in mouse brain tumor mitochondria: lipidomic evidence supporting the Warburg theory of cancer

Michael A. Kiebish,* Xianlin Han,† Hua Cheng,† Jeffrey H. Chuang,* and Thomas N. Seyfried[1,*]

Department of Biology,* Boston College, Chestnut Hill, MA; and Department of Internal Medicine,† Washington University School of Medicine, St. Louis, MO

Abstract Otto Warburg first proposed that cancer originated from irreversible injury to mitochondrial respiration, but the structural basis for this injury has remained elusive. Cardiolipin (CL) is a complex phospholipid found almost exclusively in the inner mitochondrial membrane and is intimately involved in maintaining mitochondrial functionality and membrane integrity. Abnormalities in CL can impair mitochondrial function and bioenergetics. We used shotgun lipidomics to analyze CL content and composition in highly purified brain mitochondria from the C57BL/6J (B6) and VM/Dk (VM) inbred strains and from subcutaneously grown brain tumors derived from these strains to include an astrocytoma and ependymoblastoma (B6 tumors), a stem cell tumor, and two microgliomas (VM tumors). Major abnormalities in CL content or composition were found in all tumors. The compositional abnormalities involved an abundance of immature molecular species and deficiencies of mature molecular species, suggesting major defects in CL synthesis and remodeling. The tumor CL abnormalities were also associated with significant reductions in both individual and linked electron transport chain activities. A mathematical model was developed to facilitate data interpretation. The implications of our findings to the Warburg cancer theory are discussed.— Kiebish, M. A., X. Han, H. Cheng, J. H. Chuang, and T. N. Seyfried. **Cardiolipin and electron transport chain abnormalities in mouse brain tumor mitochondria: lipidomic evidence supporting the Warburg theory of cancer. *J. Lipid Res.* 2008.** 49: **2545–2556.**

Supplementary key words metabolism • tumorigenesis • carcinogenesis • bioenergetics

Otto Warburg first proposed that the prime cause of cancer was impaired energy metabolism (1, 2). This impairment involved irreversible injury to cellular respiration that was followed in time by a gradual dependence on fermentation (glycolytic) energy to compensate for the energy lost from respiration. Cell viability requires a constant delta G′ of ATP hydrolysis of approximately −57 kJ/mol (3, 4). Most normal mammalian cells achieve this level of useable energy through respiration, whereas tumor cells achieve this level through a combination of respiration and glycolysis (2, 5). Indeed, elevated glycolysis is the metabolic hallmark of nearly all tumors, including brain tumors, and is the basis for tumor imaging using labeled glucose analogs (5–8). Much controversy has surrounded the Warburg theory, however, largely over issues regarding the Pasture effect and aerobic glycolysis (9–14). Numerous structural and biochemical abnormalities occur in tumor cell mitochondria that could compromise function, thus forcing a reliance on glycolysis for cell survival (5, 6, 9, 15–17). Although several prior studies have evaluated the lipid composition of tumor mitochondria (18–25), no prior studies have evaluated both the content and the composition of cardiolipin (CL) in highly purified mitochondria isolated from brain tumors and from their orthotopic host tissue.

CL (1,3-diphosphatidyl-*sn*-glycerol) is a complex mitochondrial-specific phospholipid that regulates numerous enzyme activities, especially those related to oxidative phosphorylation and coupled respiration (26–31). CL binds complexes I, III, IV, and V and stabilizes the super complexes (I/III/IV and II/III/IV), demonstrating an absolute requirement of CL for catalytic activity of these enzyme complexes (27, 29, 32, 33). CL restricts pumped protons within its head group domain, thus providing the structural basis for mitochondrial membrane potential and supplying protons to the ATP synthase (26, 30). The activity of respiratory enzyme complexes I and III and their linked activities are directly related to CL content (29, 34, 35). The activities of the respiratory enzyme complexes are also dependent on CL molecular species composition

This work was supported by the National Institutes of Health, Grant NS-055195, the National Cancer Institute, Grant CA-102135), and the National Institute on Aging, Grant AG-23168.

Manuscript received 18 June 2008 and in revised form 5 August 2008 and in re-revised form 13 August 2008.

Published, JLR Papers in Press, August 13, 2008.
DOI 10.1194/jlr.M800319-JLR200

[1] To whom correspondence should be addressed.
e-mail: Thomas.Seyfried@bc.edu

(30). Indeed, the degree of CL unsaturation is related to states 1–3 of respiration (31, 36). CL contains two phosphate head groups, three glycerol moieties, and four fatty acyl chains (**Fig. 1**). Almost 100 molecular species of CL were recently detected in the mitochondria from mammalian brain (37, 38). Moreover, these molecular species form a unique pattern consisting of seven major groups when arranged according to FA chain length and degree of unsaturation (38). Interestingly, the CL pattern in B6 brain mitochondria is conserved across mammalian species (37). In contrast to B6 mice, VM mice have an unusual distribution of brain CL molecular species that could relate to the high incidence of spontaneous gliomas in this strain (39).

The complexity of CL molecular species is regulated through both synthesis and remodeling. The condensation of phosphatidylglycerol and CDP-diacylglycerol produces immature CL, which contains predominantly shorter chain saturated and monounsaturated fatty acyl chains (palmitic and oleic acids). The immature CL is then remodeled to form mature CL through the coordinated activities of specific lipases and acyltransferase/transacylase, which remove and transfer, respectively, longer chain unsaturated FAs from the *sn*-2 position of donor choline and ethanolamine glycerophospholipids (39–41). We recently showed that the complex pattern of brain CL molecular species arises from a simple remodeling process involving random FA incorporation (38).

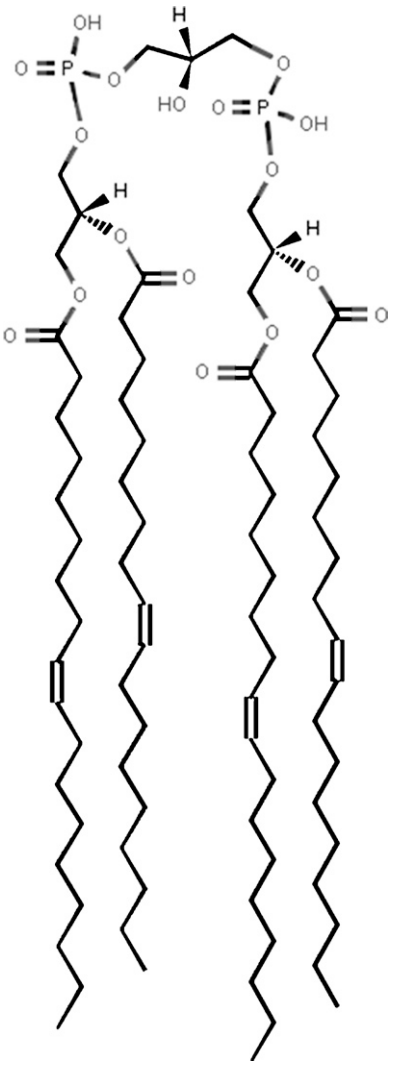

Fig. 1. Structure of cardiolipin (CL) (1,1′,2,2′-tetraoleyl cardiolipin). This is one of the over 100 CL molecular species present in mouse brain mitochondria.

Alterations in phospholipid and FA composition were previously reported in neural tumors (42–44). These alterations could influence the FAs available for CL remodeling. In the present study, we used shotgun lipidomics to analyze CL content and composition in highly purified brain mitochondria from the C57BL/6J (B6) and VM/Dk (VM) inbred strains and from subcutaneously grown brain tumors derived from these strains. The syngeneic B6 brain tumors were chemically induced and included an astrocytoma (CT-2A) and an ependymoblastoma (EPEN) (45). The syngeneic VM brain tumors arose spontaneously and included two microgliomas (VM-M2 and VM-M3) and a stem cell tumor (VM-NM1) (46). Our results show that these mouse brain tumors contain CL abnormalities that are unique to each tumor type and that these abnormalities are associated with deficiencies in electron transport chain (ETC) activities. Our results suggest that abnormal CL can underlie the irreversible respiratory injury in tumors, and they link mitochondrial lipid defects to the Warburg theory of cancer.

MATERIALS AND METHODS

Materials

Synthetic 1,1′,2,2′-tetramyristoyl cardiolipin (T14:0 CL) was purchased from Avanti Polar Lipids, Inc. (Alabaster, AL). Solvents for sample preparation and mass spectrometric analysis were obtained from Burdick and Jackson (Honeywell International, Inc., Muskegon, MI). All other chemical reagents were of at least analytical grade or the best grade available and were obtained from either Fisher Scientific (Pittsburgh, PA) or Sigma-Aldrich (St. Louis, MO).

Mice

The VM mice were obtained from Professor H. Fraser, University of Edinburgh. The B6 mice were obtained from the Jackson Laboratory (Bar Harbor, ME). Mice of both strains were matched for age (4 months) and sex (males) and were propagated under similar conditions at the Boston College Animal Facility. Mice were housed in plastic cages with filter tops containing Sani-Chip bedding (P.J. Murphy Forest Products Corp., Montville, NJ). The room was maintained at 22°C on a 12 h light/dark cycle. Food (Prolab RMH 3000; PMI LabDiet, Richmond, IN) and water were provided ad libitum. This study was conducted according to the National Institutes of Health Guide for the Care and Use of Laboratory Animals and was approved by the Institutional Animal Care Committee.

Tumors

The CT-2A and EPEN brain tumors were originally produced from the implantation of 20-methylcholanthrene in the brains of

B6 mice as previously described (45, 47). The CT-2A tumor was isolated initially from the cerebral cortex in 1985 and was characterized as a malignant anaplastic astrocytoma, whereas the EPEN tumor was isolated from the cerebral ventricle in 1949 and was characterized as an ependymoblastoma (45, 48). The VM-NM1, VM-M2, and VM-M3 tumors arose spontaneously in the cerebrum of three different adult VM mice from 1993–2000, as previously described (46). VM-NM1 is a rapidly growing nonmetastatic tumor with characteristics of neural stem cells. The VM-M2 and VM-M3 tumors are highly invasive/metastatic tumors of microglial/macrophage origin with characteristics of glioblastoma multiforme (46).

Male mice (8–12 weeks of age) were used as tumor recipients. Tumor pieces from donor mice were diced and resuspended in cold PBS at pH 7.4. Mice were anesthetized with isoflurane (Halocarbon, River Edge, NJ), and 0.1 ml of diced tumor tissue suspended in 0.2 ml PBS was implanted subcutaneously in the right flank by injection using a 1 cc tuberculin syringe and an 18 gauge needle.

Mitochondrial isolation

Nonsynaptic mouse brain or tumor mitochondria was isolated using discontinuous Ficoll and sucrose gradients as previously described (38, 39). A highly enriched mitochondrial fraction was obtained and used for lipidomics analysis as well as ETC enzyme activities.

Sample preparation for mass spectrometric analysis

An aliquot of purified mitochondria was transferred to a disposable culture borosilicate glass tube (16 mm × 100 mm). An internal standard, T14:0 CL (3 nmol/mg protein) was added to each purified mitochondrial homogenate based on the protein concentration, thereby allowing the final quantified lipid content to be normalized to the protein content to eliminate variability between the samples. Lipids from each mitochondrial homogenate were extracted by a modified Bligh and Dyer procedure as previously described (37, 49). Each lipid extract was reconstituted with a volume of 500 μl/mg protein in $CHCl_3$-MeOH (1:1; v/v). The lipid extracts were flushed with nitrogen, capped, and stored at −20°C for electrospray ionization/mass spectrometry (ESI/MS) analysis. Each lipid solution was diluted approximately 50-fold immediately prior to infusion and lipid analysis.

Instrumentation and MS

High resolution-based shotgun lipidomics analyses of CL were performed on a triple-stage quadrupole (QqQ) mass spectrometer (Thermo Scientific, San Jose, CA) equipped with an ionspray ion source as previously described (50). All ESI/MS spectrometric analyses were conducted by direct infusion, employing a Harvard syringe pump at a flow rate of 4 μl/min. Typically, 1 min or 2 min of signal averaging was employed for each mass spectrum or tandem mass spectrum, respectively. For product ion analyses by the QqQ mass spectrometer, the precursor ion was selected by the first quadrupole, with a mass window of 0.7 Th. All mass spectra and tandem mass spectra were automatically acquired by a customized sequence of sub-routines operated under Xcalibur software (51).

Electron transport chain enzyme activities

Purified mitochondrial samples were freeze-thawed three times before use in enzyme analysis to give substrate access to the inner mitochondrial membrane. All assays were performed on a temperature-controlled SpectraMax M5 plate reader (Molecular Devices) and were done in triplicate. Specific enzyme activities were calculated using ETC complex inhibitors in order to subtract background activities.

Complex I (NADH-ubiquinone oxidoreductase) activity was determined by measuring the decrease in the concentration of NADH at 340 nm as previously described (52, 53). The assay was performed in buffer containing 50 mM potassium phosphate (pH 7.4), 2 mM KCN, 5 mM $MgCl_2$, 2.5 mg/ml BSA, 2 μM antimycin, 100 μM decylubiquinone, and 0.3 mM K_2NADH. The reaction was initiated by adding purified mitochondria (20 μg). The enzyme activity was measured for 5 min, and values were recorded 30 s after the initiation of the reaction. Specific activities were determined by calculating the slope of the reaction in the linear range in the presence or absence of 1 μM rotenone (complex I inhibitor).

Complex I/III (NADH cytochrome c reductase) activity was determined by measuring the reduction of oxidized cytochrome c at 550 nm. The complex I/III assay was performed in buffer [50 mM potassium phosphate (pH 7.4), 1 mM EDTA, 2 mM KCN, 32 μM oxidized cytochrome c, and 105 μM K_2NADH] and was initiated by adding purified mitochondria (10 μg). The reaction was measured for 30 s with a linear slope in the presence or absence of 1 μM rotenone and 2 μM antimycin (complex I and III inhibitors) (52–54).

Complex II/III (succinate cytochrome c reductase) activity was measured following the reduction of oxidized cytochrome c at 550 nm. The complex II/III assay was performed in buffer [25 mM potassium phosphate (pH 7.4), 20 mM succinate, 2 mM KCN, 2 μg/ml rotenone] using purified mitochondria (10 μg). The reaction was initiated by adding 40 μM oxidized cytochrome c in the presence or absence of 2 μM antimycin (complex III inhibitor) (52, 53).

Association of mitochondrial ETC activities with CL content and composition

Because mitochondrial ETC activities depend on the content and the composition of CL, we modeled ETC activities as a function of CL content and composition in the mouse brain tumors. The two main variables included *1*) total CL content and *2*) the distribution of CL molecular species in mitochondria. The information about the molecular species distribution was simplified into a single number, which described the degree of relationship of the CL composition of the tumor mitochondria to that of brain

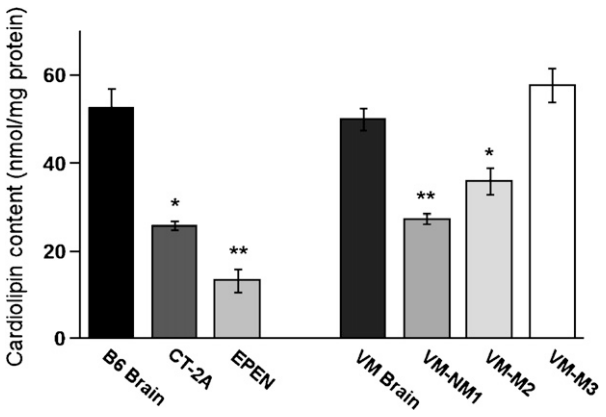

Fig. 2. CL content in mitochondria isolated from mouse brain and brain tumors. Mitochondria were isolated as described in Materials and Methods. Values are represented as the mean ± SD of three independent mitochondrial preparations from brain or tumor tissue. Asterisks indicate that the tumor values differ significantly from the B6 or the VM brain values at the * $P < 0.01$ or ** $P < 0.001$ levels as determined by the two-tailed *t*-test.

mitochondria from the host mouse strain. This number was generated as a Pearson product-moment correlation. Rather than using the correlation coefficients as a statistical measure of significance, we used the correlation coefficient only to assess the degree of "compositional similarity" of CL from the host mouse brain mitochondria to that of tumor mitochondria. A low coefficient indicates that CL molecular species composition is dissimilar between the host brain mitochondria and the tumor mitochondria. A high correlation indicates that CL molecular species composition is similar between the host brain mitochondria and the tumor mitochondria.

The following formula was used to associate each ETC activity (complex I, complex I/III, and complex II/III) with CL content and composition.

$$\text{Activity} = a_1 \text{ content} + a_2 \text{ content} \times \text{correlation} + c$$

We modeled the activity of a given ETC enzyme complex as a sum of three terms. The first term (a_1 content) is based on the assumption that ETC activity will decrease with decreases in CL content. The second term (a_2 content × correlation) is based on the assumption that ETC activity is related to both CL content and the distribution of molecular species. The third term (c) is a constant indicating a basal level of enzymatic activity independent of CL. The best-fit values of a_1, a_2, and c were calculated in the R statistical programming environment (55) for each complex using the B6 data. We then considered whether the B6 and the VM ETC activities had similar biochemical dependences on the CL content and molecular distribution. We tested this by plotting the VM data on the B6-fit quadratic surfaces. To plot the data concurrently, we shifted the VM data vertically to best fit the B6 surfaces. In other words, optimal VM c values for each complex were fit to minimize the square deviation from the B6 surfaces. This shift is necessary because the CL pattern of the VM brain is different from that of the B6 brain (39). The relative c values in the B6 and VM strains for complex I were −30.277 and −343.775, respectively. The relative c values for complex I/III were +1.306 and −115.125, respectively. The relative c values for complex II/III were +21.634 and −51.15, respectively. We found that the VM data exhibited qualitative behavior consistent with the B6-fit surfaces.

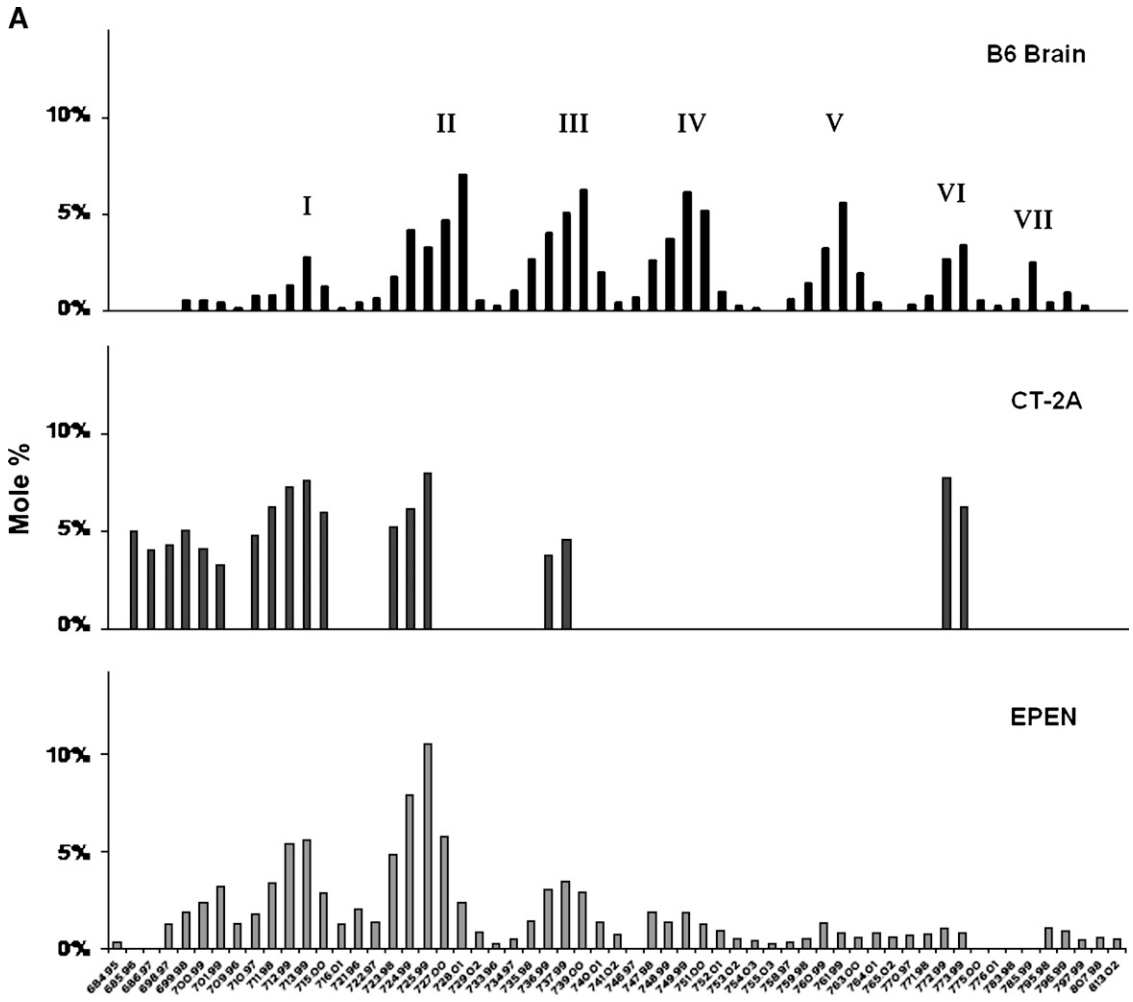

Fig. 3. Distribution of CL molecular species in mouse brain and brain tumor mitochondria. A: Distribution in B6 mouse brain and in the CT-2A and the EPEN tumors. B: Distribution in VM mouse brain and the VM-NM1, the VM-M2, and the VM-M3 tumors. CL molecular species are arranged according to the mass-to-charge ratio based on percentage distribution and are subdivided into seven major groups as we previously described (38). Corresponding mass content of molecular species in normal brain and tumor mitochondria can be found in Table 1. All values are expressed as the mean of three independent mitochondrial preparations, in which six cortexes or tumors were pooled for each preparation.

RESULTS

We used multiple discontinuous gradients to obtain highly purified mitochondria from normal brain and from brain tumor tissue. The length, as well as choice of discontinuous gradients employed, was designed for the purpose of mitochondrial lipid analysis as well as for assessment of ETC enzyme activities by standard biochemical procedures (38). We recently showed that these isolation procedures provide precise information on the content and composition of total mitochondrial lipids when analyzed using shotgun lipidomics (38, 39). Mitochondria were isolated from the brain tumors grown subcutaneously in order to avoid contamination from normal brain tissue surrounding the tumors. Because the tumors analyzed were derived from either neural stem/progenitor cells or from glial cells (45, 46, 56), the CL in tumor mitochondria was compared with that in nonsynaptic mitochondria from syngeneic mouse brain. Our analysis in purified mitochondria also eliminates issues regarding differences in mitochondrial content between tumor tissue and normal tissue (57). Because the B6 and VM mouse strains differ in CL composition (39), our comparative analysis was between the host strain and those syngeneic tumors arising in that strain.

CL abnormalities in the CT-2A and the EPEN tumors

CL content was significantly lower in the mitochondria from the CT-2A and the EPEN tumors than in the non-

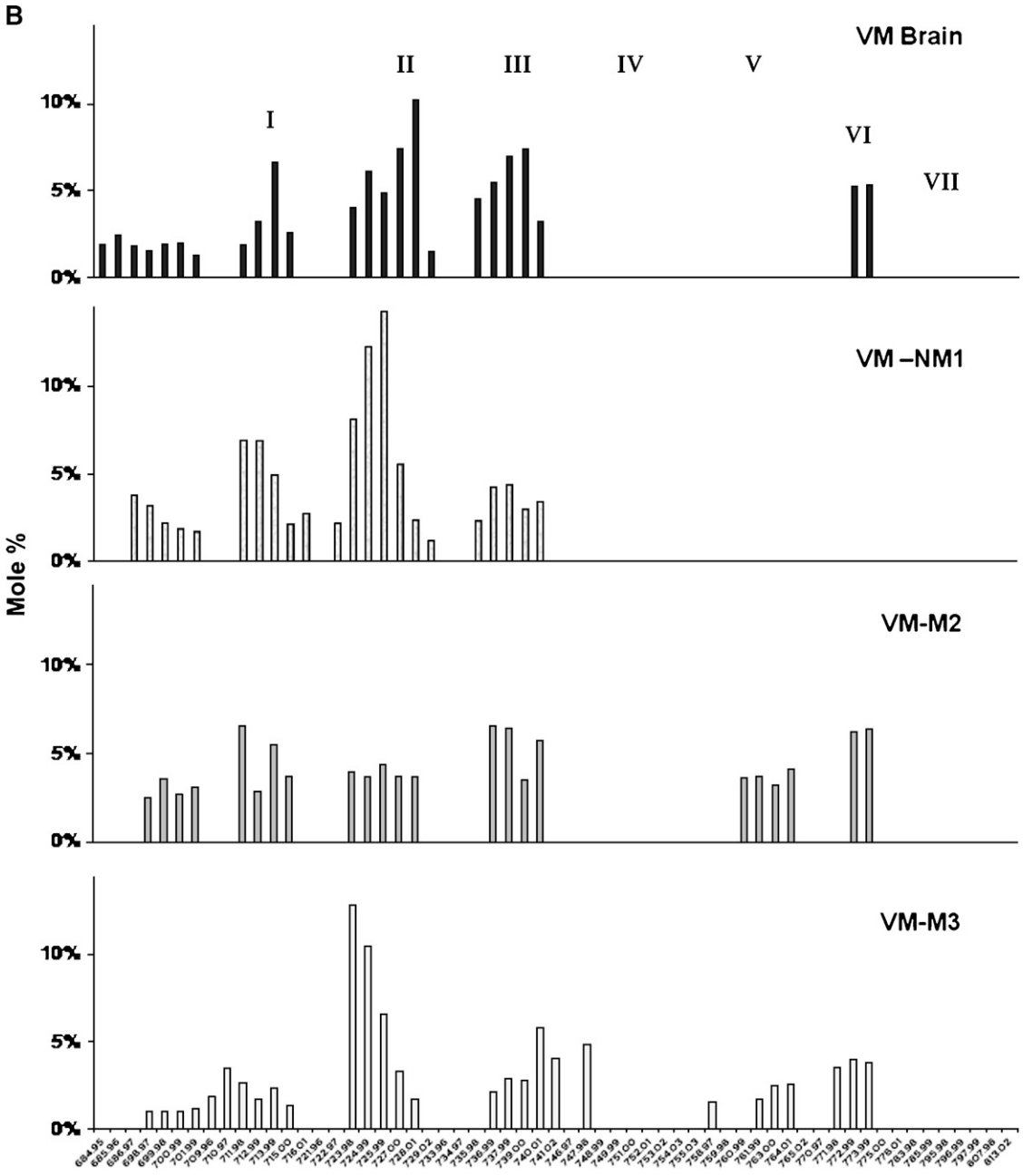

Fig. 3.—*Continued.*

TABLE 1. Mass content of cardiolipin molecular species of mitochondria isolated from brain and brain tumors

$[M-2H]^-$	Molecular Species	B6 Brain	CT-2A	EPEN	VM Brain	VM NM1	VM M2	VM M3
684.95	18:1-16:1-16:1-16:1			0.04±0.01	0.94±0.31			
685.96	18:1-16:1-16:1-16:0		1.31±0.03		1.24±0.48			
686.97	18:1-16:1-16:0-16:0		1.06±0.26		0.88±0.19	1.05±0.30		
698.97	18:2-18:1-16:1-16:1		1.14±0.12	0.17±0.01	0.77±0.29	0.88±0.02	0.92±0.11	0.59±0.14
699.98	18:1-18:1-16:1-16:1	0.30±0.03	1.33±0.34	0.26±0.05	0.95±0.14	0.63±0.05	1.29±0.08	0.58±0.12
700.99	18:1-18:1-16:0-16:1	0.31±0.05	1.08±0.23	0.32±0.07	0.97±0.35	0.51±0.09	0.97±0.17	0.59±0.21
	18:2-18:1-16:0-16:0							
	18:2-18:0-16:1-16:0							
701.99	18:1-18:1-16:0-16:0	0.24±0.04	0.87±0.17	0.44±0.11	0.65±0.29	0.47±0.03	1.14±0.17	0.67±0.25
	18:2-18:0-16:0-16:0							
	18:1-18:0-16:0-16:1							
709.96	20:4-18:2-16:1-16:1	0.09±0.01		0.17±0.07				1.03±0.39
710.97	20:4-18:1-16:1-16:1	0.41±0.06	1.25±0.17	0.24±0.01				2.02±0.12
	20:4-18:2-16:1-16:0							
711.98	20:4-18:1-16:1-16:0	0.45±0.06	1.62±0.11	0.46±0.09	0.95±0.28	1.91±0.02	2.35±0.16	1.51±0.23
	18:2-18:2-18:1-16:1							
712.99	18:2-18:1-18:1-16:1	0.71±0.02	1.91±0.07	0.73±0.17	1.62±0.05	1.92±0.11	1.04±0.15	1.00±0.19
	18:1-18:1-18:1-16:2							
	18:2-18:1-18:0-16:2							
	18:2-18:2-18:0-16:1							
713.99	18:1-18:1-18:1-16:1	1.47±0.23	2.00±0.63	0.75±0.15	3.34±0.73	1.35±0.08	1.99±0.31	1.33±0.20
	18:2-18:1-18:1-16:0							
715.00	18:1-18:1-18:1-16:0	0.68±0.04	1.57±0.30	0.39±0.08	1.30±0.09	0.59±0.08	1.34±0.08	0.76±0.15
	18:0-18:1-18:1-16:1							
716.01	18:0-18:1-18:1-16:0	0.09±0.02		0.17±0.05		0.76±0.43		
	18:0-18:0-18:1-16:1							
721.96	20:4-20:4-16:1-16:1	0.23±0.03		0.27±0.08				
722.97	20:4-20:4-16:1-16:0	0.36±0.03		0.18±0.05		0.60±0.10		
	20:4-18:2-18:2-16:1							
723.98	20:4-18:2-18:1-16:1	0.95±0.08	1.36±0.21	0.65±0.14	2.01±0.13	2.24±0.19	1.42±0.32	7.42±1.09
724.99	20:4-18:2-18:1-16:0	2.22±0.17	1.61±0.31	1.07±0.19	3.08±0.34	3.38±0.14	1.35±0.11	6.07±0.44
	20:4-18:1-18:1-16:1							
725.99	20:4-18:1-18:1-16:0	1.74±0.13	2.09±0.04	1.42±0.31	2.46±0.26	3.93±0.29	1.58±0.05	3.83±0.65
	20:3-18:1-18:1-16:1							
727.00	18:2-18:1-18:1-18:1	2.48±0.33		0.77±0.15	3.73±0.18	1.52±0.13	1.35±0.40	1.90±0.22
728.01	18:1-18:1-18:1-18:1	3.72±0.72		0.32±0.05	5.13±0.95	0.65±0.09	1.33±0.33	0.97±0.17
729.02	18:1-18:1-18:1-18:0	0.30±0.03		0.11±0.03	0.75±0.26	0.33±0.06		
733.96	22:6-20:4-16:1-16:1	0.14±0.02		0.04±0.01				
734.97	20:4-20:4-18:2-16:1	0.56±0.06		0.07±0.02				
735.98	20:4-20:4-18:1-16:1	1.41±0.16		0.20±0.05	2.29±0.67	0.63±0.11		
736.99	20:4-20:4-18:1-16:0	2.11±0.07	1.00±0.07	0.41±0.14	2.78±0.42	1.18±0.10	2.38±0.62	1.23±0.26
	22:6-18:1-18:1-16:1							
	22:6-18:2-18:1-16:0							
737.99	20:4-18:2-18:1-18:1	2.68±0.37	1.20±0.28	0.46±0.10	3.52±0.65	1.21±0.25	2.32±0.54	1.67±0.26
	22:6-18:1-18:1-16:0							
739.00	20:4-18:1-18:1-18:1	3.30±0.45		0.39±0.11	3.71±0.45	0.81±0.08	1.27±0.15	1.61±0.25
740.01	20:4-18:1-18:1-18:0	1.07±0.14		0.19±0.04	1.62±0.30	0.94±0.38	2.08±0.85	3.35±0.62
	20:3-18:1-18:1-18:1							
741.02	20:4-18:1-18:0-18:0	0.25±0.08		0.10±0.02				2.34±0.30
	20:3-18:1-18:1-18:0							
746.97	22:6-18:3-18:2-18:2	0.40±0.04						
747.98	20:4-20:4-18:2-18:2	1.38±0.09		0.25±0.04				2.81±0.47
	20:4-20:4-20:4-16:0							
	22:6-20:4-18:1-16:1							
	22:6-22:6-16:0-16:0							
	22:6-18:2-18:2-18:2							
748.99	20:4-20:4-18:2-18:1	1.99±0.19		0.19±0.03				
749.99	20:4-20:4-18:1-18:1	3.24±0.24		0.26±0.04				
751.00	22:6-18:1-18:1-18:1	2.74±0.10		0.17±0.02				
	20:4-20:3-18:1-18:1							
752.01	22:6-18:1-18:1-18:0	0.54±0.17		0.12±0.04				
753.02	20:4-20:2-18:1-18:0	0.15±0.04		0.07±0.01				
	20:4-20:1-18:1-18:1							
754.03	20:4-20:1-18:1-18:0	0.09±0.02		0.05±0.02				
755.03	20:4-20:1-18:0-18:0			0.04±0.01				
758.97	22:6-20:4-20:4-16:1	0.32±0.04		0.05±0.02				0.89±0.19
	22:6-22:6-18:2-16:1							
759.98	22:6-20:4-18:2-18:2	0.76±0.05		0.07±0.03				
	22:6-20:4-20:4-16:0							
	22:6-22:6-18:1-16:1							

(continued)

TABLE 1. Continued

$[M-2H]^-$	Molecular Species	B6 Brain	CT-2A	EPEN	VM Brain	VM NM1	VM M2	VM M3
760.99	22:6-20:4-18:2-18:1	1.72±0.08		0.18±0.08			1.31±0.32	
761.99	22:6-20:4-18:1-18:1	2.94±0.23		0.11±0.02			1.35±0.15	0.97±0.16
763.00	22:6-20:4-18:1-18:0	1.03±0.05		0.07±0.02			1.16±0.26	1.45±0.22
	22:6-20:3-18:1-18:1							
764.01	22:4-20:4-18:1-18:1	0.24±0.02		0.11±0.03			1.48±0.33	1.47±0.24
	22:6-20:3-18:1-18:0							
765.02	22:4-20:4-18:1-18:0			0.08±0.01				
770.97	22:6-20:4-20:4-18:3	0.18±0.05		0.09±0.02				
771.98	22:6-22:6-20:4-16:0	0.42±0.05		0.10±0.04				2.04±0.23
	20:4-20:4-20:4-20:4							
	22:6-20:4-20:4-18:2							
	22:6-22:6-18:2-18:2							
772.99	22:6-20:4-20:4-18:1	1.42±0.12	2.03±0.11	0.14±0.04	2.65±0.12		2.25±0.45	2.32±0.31
773.99	22:6-22:6-18:1-18:1	1.81±0.09	1.64±0.18	0.11±0.02	2.68±0.10		2.30±0.99	2.22±0.42
	22:6-20:4-20:3-18:1							
775.00	16:0-20:3-22:5-22:5	0.28±0.10						
	18:2-20:3-20:3-22:5							
	18:0-18:1-22:6-22:6							
	18:0-20:3-20:4-22:6							
776.01	18:0-18:0-22:6-22:6	0.16±0.05						
783.98	22:6-22:6-20:4-18:2	0.33±0.05						
785.99	22:6-22:6-20:4-18:1	1.34±0.08						
	22:6-20:4-20:4-20:3							
795.98	20:4-20:4-22:6-22:6	0.25±0.09		0.14±0.06				
796.99	22:6-22:6-22:6-18:1	0.50±0.04		0.12±0.05				
	22:6-22:6-20:4-20:3							
797.99	20:4-20:3-22:6-22:5	0.16±0.07		0.06±0.02				
	22:6-22:6-22:6-18:0							
	22:6-22:6-22:5-18:1							
807.98	20:4-22:6-22:6-22:6			0.07±0.03				
813.02	22:6-22:6-22:6-22:5			0.06±0.02				

Lipid extracts from purified mitochondria were prepared using a modified Bligh and Dyer procedure. The cardiolipin (CL) molecular species in the lipid extracts were identified by searching for plus-one isotopologues of double-charged CL ions followed by product-ion analyses of these plus-one isotopologues. The CL molecular mass was obtained from the quadrupole mass spectrometer (QqQ) mass spectrometer. The doubly charged CL plus-one isotopologues were used to quantify individual CL molecular species as previously described (50, 73). The results are expressed as nmol/mg protein and represent the mean ± standard deviation from three independent isolations of mitochondria. The ion peaks of CL molecular species that constituted less than 0.01 nmol/mg protein as determined by a QqQ mass spectrometer have been omitted from the Table.

synaptic mitochondria from the control B6 mouse brain (**Fig. 2**). Almost 100 molecular species of CL occur in nonsynaptic mitochondria from B6 mice (38). When arranged according to mass-to-charge ratios, these molecular species form a unique pattern consisting of seven major groups (**Fig. 3A** and **Table 1**). Group I contains predominantly shorter chain saturated or monounsaturated FAs, whereas groups V–VII contain predominantly longer chain PUFAs (38). The shorter chain saturated or monounsaturated FAs are indicative of immature CL, whereas the longer chain PUFAs are indicative of mature CL. The distribution of CL molecular species in the CT-2A and the EPEN mitochondria differed markedly from that of the B6 nonsynaptic mitochondria (Fig. 3A). The degree of relationship in CL molecular species distribution, expressed as a correlation coefficient between B6 nonsynaptic mitochondria and CT-2A and EPEN tumor mitochondria, was 0.098 and 0.419, respectively. CT-2A was missing most molecular species in groups IV, V, and VII, while also expressing an abundance of species in and around group I. The distribution of CL molecular species was also abnormal in groups II, III, and VI. As with the CL distribution in CT-2A mitochondria, the CL distribution in the EPEN mitochondria also contained an abundance of species in and around group I and deficiency of species in groups III–VII. The overall distribution of molecular species also differed between the CT-2A and EPEN tumors.

CL abnormalities in the VM-M2, VM-M3, and VM-NM1 tumors

In contrast to the B6 mouse brain, which contains about 100 molecular species of CL symmetrically distributed over seven major groups (Fig. 3A), the VM mouse brain is unique in having only about 45 major CL molecular species and in missing molecular species in groups IV, V, and VII (Fig. 3B and Table 1). CL content was significantly lower in the mitochondria from the VM-NM1 and the VM-M2 tumors than in the nonsynaptic mitochondria from the control VM mouse brain (Fig. 2). No significant difference in CL content was found between the VM-M3 tumor and the VM brain. Each VM tumor differed from the VM brain with respect to the distribution of CL molecular species (Fig. 3B). The degree of relationship in CL molecular species distribution, expressed as a correlation coefficient between VM nonsynaptic mitochondria and the VM-NM1, VM-M2, and VM-M3 tumor tissue, was 0.601, 0.699, and 0.475, respectively. The CL molecular species also differed significantly among the VM tumors.

Electron transport abnormalities in mouse brain tumors

The activities of complexes I, I/III, and II/III were significantly lower in mitochondria from the CT-2A and the EPEN tumors than in mitochondria from the syngeneic B6 brain. Likewise, these ETC activities were significantly lower in mitochondria from the VM-NM1, VM-M2, and VM-M3 brain tumors than in mitochondria from the syngeneic VM brain (**Fig. 4**). The unusual distribution of CL molecular species in the VM brain mitochondria could account for the lower ETC activities in the VM mice, compared with the B6 mice, as we recently described (39).

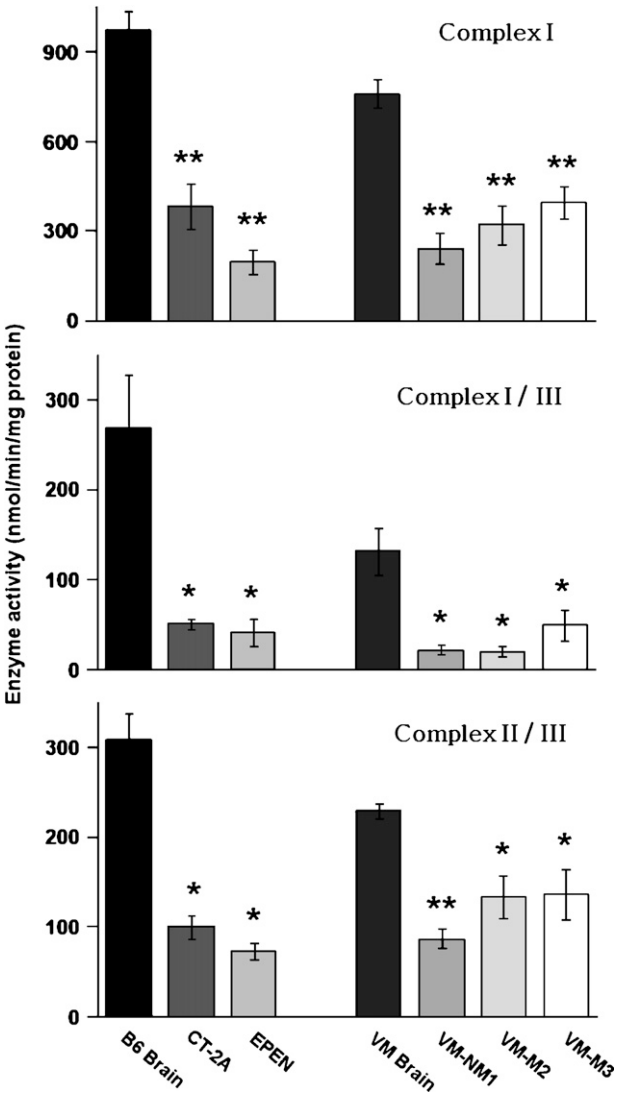

Fig. 4. Electron transport chain (ETC) enzyme activities of complexes I, I/III, and II/III in mouse brain and brain tumor mitochondria. Enzyme activities are expressed as nmol/min/mg protein as described in Materials and Methods. All values are expressed as the mean of three to four independent mitochondrial preparations, in which six cortexes or tumors were pooled for each preparation. Asterisks indicate that the tumor values differ significantly from the B6 or the VM brain values at the * $P < 0.025$ or ** $P < 0.001$ levels as determined by the two-tailed *t*-test.

Relationship of CL abnormalities to ETC activities in the B6 and the VM brain tumors

To illustrate the relationship of ETC enzyme activities to CL content and composition, we utilized a two-dimensional linear regression to fit the measured activity values to a function of the form: activity = a_1 content + a_2 content × correlation + c (see Materials and Methods). The best-fit relationship for each complex was expressed as a quadratic surface. Our objective was to compare the data for the CT-2A and the EPEN tumors with those for their B6 host strain and to compare the VM-NM1, VM-M2, and VM-M3 tumors with their VM host strain. This analysis demonstrated a direct relationship between ETC activity, CL content, and the distribution of molecular species (**Fig. 5**). In comparing the B6 tumors with their host strain for complex I, the quadratic surface was calculated as: activity = 15.614 content + 3.443 content × correlation −30.277. For complex I/III, the quadratic surface was calculated as: activity = 1.599 content + 3.480 content × correla-

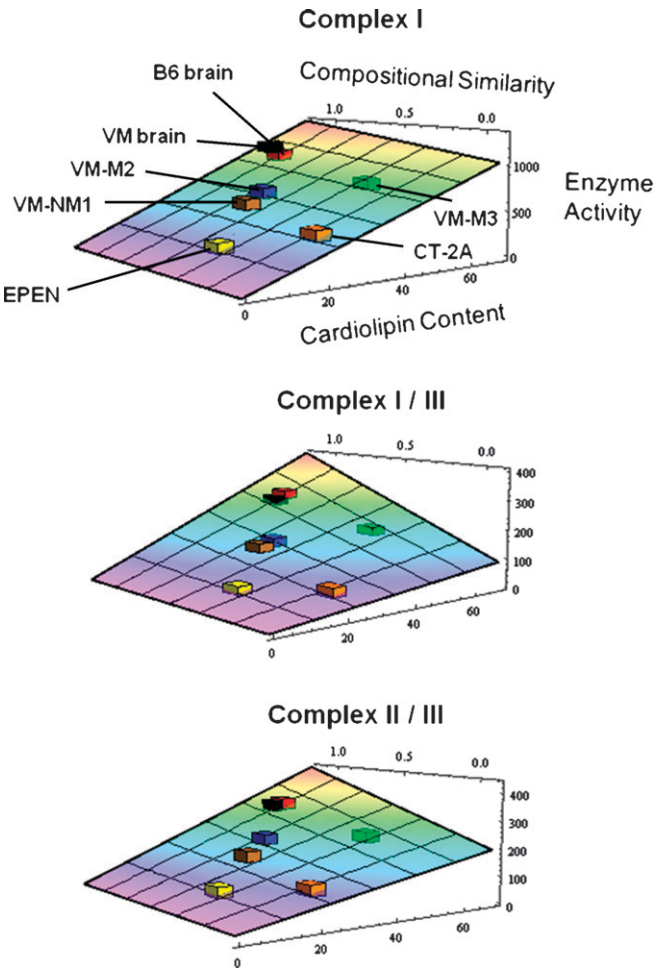

Fig. 5. Relationship of CL abnormalities to ETC activities in the B6 and the VM mouse brain tumors. The data are expressed on the best-fit three-dimensional quadratic surface for each electron transport chain complex as described in Materials and Methods. To illustrate the position of all tumors on the same graph relative to their host strain, the data for the VM strain and tumors were fit to the B6-fit quadratic surface as described in Materials and Methods.

tion + 1.306. For complex II/III, the quadratic surface was calculated as: activity = 2.768 content + 2.685 content × correlation + 21.634. For each complex, the ETC activity decreased with decreases in CL content relative to that in the B6 brain. However, the a_1 component was greater for complex I (15.614) than for complex I/III (1.599) or complex II/III (2.768), indicating that complex I activity is more dependent on CL content than is the activity of the other two complexes. Similar trends were also found for the relationship between ETC activities and CL abnormalities in the VM brain tumors.

The various tumors cover a variety of CL contents and molecular species compositions, suggesting that the enzymatic activity surfaces that we have modeled will be useful for predicting complex activities in other tumors using CL content and distribution. For example, the EPEN tumor was positioned furthest from its control B6 host strain, whereas the VM-M3 tumor was positioned closest to its VM host strain. These data demonstrate that the difference between a tumor and its respective host strain for an ETC activity is directly related to the difference between the tumor and host in CL content and composition.

DISCUSSION

The Warburg theory describes cancer as a metabolic disease of cellular respiration and has generated considerable debate and controversy in the cancer field. Much of the controversy surrounds the molecular mechanisms responsible for aerobic glycolysis, which involves defects in the Pasture effect (13, 14, 58, 59). Indeed, the expression of aerobic glycolysis in tumor cells has become generally known as the "Warburg effect" (10, 11, 60). Interestingly, Warburg considered the phenomenon of aerobic glycolysis as too labile or too dependent on environmental conditions to be a reliable indicator of tumor metabolism (1, 2). Rather, he emphasized the importance of structural defects in respiration as the more robust mechanism of cancer. A greater dependence on glycolysis would naturally arise following irreversible respiratory injury in order to maintain an adequate delta G′ of ATP hydrolysis for cell survival. The emphasis on disturbances in aerobic glycolysis has diverted attention away from the key aspect of Warburg's theory on the underlying structural abnormalities responsible for injured respiration in tumor cells (9, 12, 60). Because CL is a major structural lipid of the mitochondrial inner membrane that influences mitochondrial function and bioenergetics, we investigated for the first time the content and composition of CL in highly purified mitochondria from a diverse group of mouse brain tumors.

We found that CL composition and/or content in mouse brain tumor mitochondria differed markedly from that in mitochondria derived from the normal syngeneic host brain tissue. Moreover, we showed that these CL abnormalities were associated with significant reductions in ETC activities, consistent with the pivotal role of CL in maintaining the structural integrity of the inner mitochondrial membrane (31). We conducted our studies on mitochondria isolated from brain tumors grown in vivo rather than on mitochondria isolated from cultured brain tumor cells, because our preliminary studies showed that in vitro culture conditions produce CL abnormalities that would confound data interpretation (61). Our findings of CL abnormalities in five diverse mouse brain tumor types are consistent with earlier studies in rat hepatomas showing shorter chain saturated FAs (palmitic and stearic) characteristic of immature CL (22, 62). On the basis of these and other observations, we suggest that most tumors, regardless of cell origin, contain abnormalities in CL composition and/or content.

Because ETC complexes I, I/III, and II/III are necessary for maintaining the mitochondrial proton gradient and

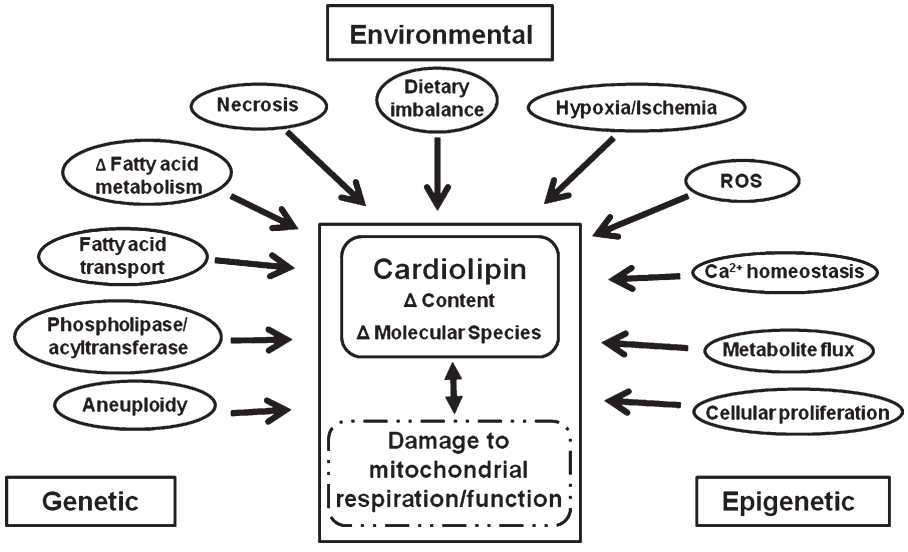

Fig. 6. Relationship of genetic, epigenetic, and environmental factors to dysfunctional respiration associated with abnormalities in CL content and composition. ROS, reactive oxygen species.

respiratory energy production (26, 63), the CL abnormalities we found will compromise respiratory energy metabolism in these brain tumors. Moreover, we consider it highly unlikely that the CL abnormalities expressed in the various mouse brain tumors, or in any tumor for that matter, are reversible. The correction of CL abnormalities in tumors would require a cession of tumor growth coupled with multiple changes in CL synthesis and remodeling. Owing to the complex nature of CL remodeling as well as to the multiple components involved (41), it seems unlikely that CL molecular speciation could be restored in any cancer cell. Hence, our findings in mouse brain tumors provide evidence linking abnormal CL to irreversible respiratory injury.

Although Warburg emphasized that irreversible respiratory injury was the prime cause of cancer, it is unclear whether the CL abnormalities we found in these mouse brain tumors arose as a cause or as an effect of tumorigenesis or tumor progression. Originally, the CT-2A astrocytoma and EPEN ependymoblastoma arose many months after 20-methylcholantherene implantation in the B6 mouse brain, whereas the VM tumors arose spontaneously in the brains of adult VM mice (45, 46). The brain tumors we studied were grown from clonal cell lines established from each tumor. The high reproducibility of the CL abnormalities within independent samples indicates that the CL abnormalities are a stable phenotype of each brain tumor type. The ETC abnormalities in these mouse brain tumors do not arise from mutations within the mitochondrial genome, because no pathogenic mutations were found in the sequenced genome of each brain tumor (64). It is interesting, however, that abnormalities in CL molecular species exist in the brains of the inbred VM mice (39). These CL abnormalities might contribute to the relatively high incidence of spontaneous gliomas in this strain. In light of these findings, we suggest that inherited mutations within the nuclear genome could contribute either directly or indirectly to abnormalities in CL synthesis or remodeling.

In addition to inherited mutations, somatic mutations in tumor suppressor/oncogenes or aneuploidy could also produce mitochondrial defects, thus causing CL abnormalities (65–67). CL abnormalities could also arise from a variety of epigenetic causes involving abnormalities in cellular proliferation, metabolic flux, and calcium homeostasis (68–70). A variety of environmental insults, including necrosis, hypoxia/ischemia, dietary imbalances, and reactive oxygen species, could also alter CL content and/or composition, thus contributing to tumor initiation or progression (71–75). Hence, respiratory injury in tumor cells can be linked to CL abnormalities through numerous genetic, epigenetic, and environmental factors (**Fig. 6**).

The CL abnormalities we describe here could underlie in part the therapeutic response of these and other tumors to dietary energy restriction and metabolic targeting (4, 76–82). By impairing ETC efficiency, CL abnormalities would reduce the ability of tumor cells to obtain energy from metabolic fuels other than glucose (3). Although our findings provide evidence linking the Warburg cancer theory with abnormal CL, it is important to recognize that not all CL abnormalities are associated with cancer. Indeed, CL abnormalities have been found in a variety of non-neoplastic diseases, to include diabetes, Barth syndrome, and several neurodegenerative diseases (40, 73, 74). Nevertheless, our findings provide new evidence that abnormal CL can underlie the irreversible respiratory injury in tumors, thus linking Warburg's cancer theory to abnormal CL.

The authors would like to thank Mary Roberts, Daniel Kirschner, Rena Baek, Purna Mukherjee, and John Mantis for helpful discussions.

REFERENCES

1. Warburg, O. 1931. The Metabolism of Tumours. Richard R. Smith, Inc., New York.
2. Warburg, O. 1956. On the origin of cancer cells. *Science.* **123:** 309–314.
3. Veech, R. L. 2004. The therapeutic implications of ketone bodies: the effects of ketone bodies in pathological conditions: ketosis, ketogenic diet, redox states, insulin resistance, and mitochondrial metabolism. *Prostaglandins Leukot. Essent. Fatty Acids.* **70:** 309–319.
4. Seyfried, T. N., and P. Mukherjee. 2005. Targeting energy metabolism in brain cancer: review and hypothesis. *Nutr. Metab. (Lond).* **2:** 30.
5. Wu, M., A. Neilson, A. L. Swift, R. Moran, J. Tamagnine, D. Parslow, S. Armistead, K. Lemire, J. Orrell, J. Teich, et al. 2007. Multiparameter metabolic analysis reveals a close link between attenuated mitochondrial bioenergetic function and enhanced glycolysis dependency in human tumor cells. *Am. J. Physiol. Cell Physiol.* **292:** C125–C136.
6. Oudard, S., E. Boitier, L. Miccoli, S. Rousset, B. Dutrillaux, and M. F. Poupon. 1997. Gliomas are driven by glycolysis: putative roles of hexokinase, oxidative phosphorylation and mitochondrial ultrastructure. *Anticancer Res.* **17:** 1903–1911.
7. Galarraga, J., D. J. Loreck, J. F. Graham, R. L. DeLaPaz, B. H. Smith, D. Hallgren, and C. J. Cummins. 1986. Glucose metabolism in human gliomas: correspondence of in situ and in vitro metabolic rates and altered energy metabolism. *Metab. Brain Dis.* **1:** 279–291.
8. Kirsch, W. M., Q. Schulz, J. Van Buskirk, and P. Nakane. 1972. Anaerobic energy metabolism in brain tumors. *Prog. Exp. Tumor Res.* **17:** 163–191.
9. Colowick, S. P. 1961. The status of Warburg's theory of glycolysis and respiration in tumors. *Q. Rev. Biol.* **36:** 273–276.
10. Gatenby, R. A., and R. J. Gillies. 2004. Why do cancers have high aerobic glycolysis? *Nat. Rev. Cancer.* **4:** 891–899.
11. Busk, M., M. R. Horsman, P. E. Kristjansen, A. J. van der Kogel, J. Bussink, and J. Overgaard. 2008. Aerobic glycolysis in cancers: implications for the usability of oxygen-responsive genes and fluorodeoxyglucose-PET as markers of tissue hypoxia. *Int. J. Cancer.* **122:** 2726–2734.
12. Gogvadze, V., S. Orrenius, and B. Zhivotovsky. 2008. Mitochondria in cancer cells: what is so special about them? *Trends Cell Biol.* **18:** 165–173.
13. Weinhouse, S. 1976. The Warburg hypothesis fifty years later. *Z. Krebsforsch. Klin. Onkol. Cancer Res. Clin. Oncol.* **87:** 115–126.
14. Aisenberg, A. C. 1961. The Glycolysis and Respiration of Tumors. Academic Press, New York.
15. Foster, C. S., P. E. Spoerri, P. Glees, and O. Spoerri. 1978. The mode of mitochondrial degeneration in gliomas. *Acta Neurochir. (Wien).* **43:** 229–237.
16. Arismendi-Morillo, G. J., and A. V. Castellano-Ramirez. 2008. Ultrastructural mitochondrial pathology in human astrocytic tumors: potentials implications pro-therapeutics strategies. *J. Electron Microsc. (Tokyo).* **57:** 33–39.
17. Lopez-Rios, F., M. Sanchez-Arago, E. Garcia-Garcia, A. D. Ortega, J. R. Berrendero, F. Pozo-Rodriguez, A. Lopez-Encuentra, C. Ballestin, and J. M. Cuezva. 2007. Loss of the mitochondrial bioenergetic capacity underlies the glucose avidity of carcinomas. *Cancer Res.* **67:** 9013–9017.
18. Baggetto, L. G., E. Clottes, and C. Vial. 1992. Low mitochondrial

proton leak due to high membrane cholesterol content and cytosolic creatine kinase as two features of the deviant bioenergetics of Ehrlich and AS30-D tumor cells. *Cancer Res.* **52:** 4935–4941.
19. Bergelson, L. D., E. V. Dyatlovitskaya, I. B. Sorokina, and N. P. Gorkova. 1974. Phospholipid composition of mitochondria and microsomes from regenerating rat liver and hepatomas of different growth rate. *Biochim. Biophys. Acta.* **360:** 361–365.
20. Bergelson, L. D., E. V. Dyatlovitskaya, T. I. Torkhovskaya, I. B. Sorokina, and N. P. Gorkova. 1970. Phospholipid composition of membranes in the tumor cell. *Biochim. Biophys. Acta.* **210:** 287–298.
21. Feo, F., R. A. Canuto, G. Bertone, R. Garcea, and P. Pani. 1973. Cholesterol and phospholipid composition of mitochondria and microsomes isolated from morris hepatoma 5123 and rat liver. *FEBS Lett.* **33:** 229–232.
22. Canuto, R. A., M. E. Biocca, G. Muzio, and M. U. Dianzani. 1989. Fatty acid composition of phospholipids in mitochondria and microsomes during diethylnitrosamine carcinogenesis in rat liver. *Cell Biochem. Funct.* **7:** 11–19.
23. Hostetler, K. Y., B. D. Zenner, and H. P. Morris. 1976. Abnormal membrane phospholipid content in subcellular fractions from the Morris 7777 hepatoma. *Biochim. Biophys. Acta.* **441:** 231–238.
24. Hostetler, K. Y., B. D. Zenner, and H. P. Morris. 1979. Phospholipid content of mitochondrial and microsomal membranes from Morris hepatomas of varying growth rates. *Cancer Res.* **39:** 2978–2983.
25. Morton, R., C. Cunningham, R. Jester, M. Waite, N. Miller, and H. P. Morris. 1976. Alteration of mitochondrial function and lipid composition in Morris 7777 hepatoma. *Cancer Res.* **36:** 3246–3254.
26. Haines, T. H., and N. A. Dencher. 2002. Cardiolipin: a proton trap for oxidative phosphorylation. *FEBS Lett.* **528:** 35–39.
27. Fry, M., and D. E. Green. 1980. Cardiolipin requirement by cytochrome oxidase and the catalytic role of phospholipid. *Biochem. Biophys. Res. Commun.* **93:** 1238–1246.
28. Fry, M., G. A. Blondin, and D. E. Green. 1980. The localization of tightly bound cardiolipin in cytochrome oxidase. *J. Biol. Chem.* **255:** 9967–9970.
29. Fry, M., and D. E. Green. 1981. Cardiolipin requirement for electron transfer in complex I and III of the mitochondrial respiratory chain. *J. Biol. Chem.* **256:** 1874–1880.
30. Chicco, A. J., and G. C. Sparagna. 2007. Role of cardiolipin alterations in mitochondrial dysfunction and disease. *Am. J. Physiol. Cell Physiol.* **292:** C33–C44.
31. Hoch, F. L. 1992. Cardiolipins and biomembrane function. *Biochim. Biophys. Acta.* **1113:** 71–133.
32. McKenzie, M., M. Lazarou, D. R. Thorburn, and M. T. Ryan. 2006. Mitochondrial respiratory chain supercomplexes are destabilized in Barth Syndrome patients. *J. Mol. Biol.* **361:** 462–469.
33. Shinzawa-Itoh, K., H. Aoyama, K. Muramoto, H. Terada, T. Kurauchi, Y. Tadehara, A. Yamasaki, T. Sugimura, S. Kurono, K. Tsujimoto, et al. 2007. Structures and physiological roles of 13 integral lipids of bovine heart cytochrome c oxidase. *EMBO J.* **26:** 1713–1725.
34. Zhang, M., E. Mileykovskaya, and W. Dowhan. 2002. Gluing the respiratory chain together. Cardiolipin is required for supercomplex formation in the inner mitochondrial membrane. *J. Biol. Chem.* **277:** 43553–43556.
35. Pfeiffer, K., V. Gohil, R. A. Stuart, C. Hunte, U. Brandt, M. L. Greenberg, and H. Schagger. 2003. Cardiolipin stabilizes respiratory chain supercomplexes. *J. Biol. Chem.* **278:** 52873–52880.
36. Hoch, F. L. 1998. Cardiolipins and mitochondrial proton-selective leakage. *J. Bioenerg. Biomembr.* **30:** 511–532.
37. Cheng, H., D. J. Mancuso, X. Jiang, S. Guan, J. Yang, K. Yang, G. Sun, R. W. Gross, and X. Han. 2008. Shotgun lipidomics reveals the temporally dependent, highly diversified cardiolipin profile in the mammalian brain: temporally coordinated postnatal diversification of cardiolipin molecular species with neuronal remodeling. *Biochemistry.* **47:** 5869–5880.
38. Kiebish, M. A., X. Han, H. Cheng, A. Lunceford, C. F. Clarke, H. Moon, J. H. Chuang, and T. N. Seyfried. 2008. Lipidomic analysis and electron transport chain activities in C57BL/6J mouse brain mitochondria. *J. Neurochem.* **106:** 299–312.
39. Kiebish, M. A., X. Han, H. Cheng, J. H. Chuang, and T. N. Seyfried. 2008. Brain mitochondrial lipid abnormalities in mice susceptible to spontaneous gliomas. *Lipids.* **43:** 951–959.
40. Schlame, M., and M. Ren. 2006. Barth syndrome, a human disorder of cardiolipin metabolism. *FEBS Lett.* **580:** 5450–5455.
41. Hauff, K. D., and G. M. Hatch. 2006. Cardiolipin metabolism and Barth Syndrome. *Prog. Lipid Res.* **45:** 91–101.
42. Campanella, R. 1992. Membrane lipids modifications in human gliomas of different degree of malignancy. *J. Neurosurg. Sci.* **36:** 11–25.
43. Yates, A. J., D. K. Thompson, C. P. Boesel, C. Albrightson, and R. W. Hart. 1979. Lipid composition of human neural tumors. *J. Lipid Res.* **20:** 428–436.
44. Murphy, E. J., and L. A. Horrocks. 1993. Effects of differentiation on the phospholipid and phospholipid fatty acid composition of N1E-115 neuroblastoma cells. *Biochim. Biophys. Acta.* **1167:** 131–136.
45. Seyfried, T. N., M. el-Abbadi, and M. L. Roy. 1992. Ganglioside distribution in murine neural tumors. *Mol. Chem. Neuropathol.* **17:** 147–167.
46. Huysentruyt, L. C., P. Mukherjee, D. Banerjee, L. M. Shelton, and T. N. Seyfried. 2008. Metastatic cancer cells with macrophage properties: evidence from a new murine tumor model. *Int. J. Cancer.* **123:** 73–84.
47. Zimmerman, H. M., and H. Arnould. 1941. Experimental brain tumors: I. Tumors produced with methylcholanthrene. *Cancer Res.* **1:** 919–938.
48. Rubin, R., and C. Sutton. 1968. The ultrastructure of the mouse ependymoblastoma and its contained virus-like particles. *J. Neuropathol. Exp. Neurol.* **27:** 136.
49. Bligh, E. G., and W. J. Dyer. 1959. A rapid method of total lipid extraction and purification. *Can. J. Biochem. Physiol.* **37:** 911–917.
50. Han, X., K. Yang, J. Yang, H. Cheng, and R. W. Gross. 2006. Shotgun lipidomics of cardiolipin molecular species in lipid extracts of biological samples. *J. Lipid Res.* **47:** 864–879.
51. Han, X., J. Yang, H. Cheng, H. Ye, and R. W. Gross. 2004. Toward fingerprinting cellular lipidomes directly from biological samples by two-dimensional electrospray ionization mass spectrometry. *Anal. Biochem.* **330:** 317–331.
52. Ellis, C. E., E. J. Murphy, D. C. Mitchell, M. Y. Golovko, F. Scaglia, G. C. Barcelo-Coblijn, and R. L. Nussbaum. 2005. Mitochondrial lipid abnormality and electron transport chain impairment in mice lacking alpha-synuclein. *Mol. Cell. Biol.* **25:** 10190–10201.
53. Birch-Machin, M. A., and D. M. Turnbull. 2001. Assaying mitochondrial respiratory complex activity in mitochondria isolated from human cells and tissues. *Methods Cell Biol.* **65:** 97–117.
54. Degli Esposti, M. 2001. Assessing functional integrity of mitochondria in vitro and in vivo. *Methods Cell Biol.* **65:** 75–96.
55. R Development Core Team. 2005. R: A language and environment for statistical computing. R Foundation for Statistical Computing, Vienna, Austria.
56. Seyfried, N. T., L. C. Huysentruyt, J. A. Atwood III, Q. Xia, T. N. Seyfried, and R. Orlando. 2008. Up-regulation of NG2 proteoglycan and interferon-induced transmembrane proteins 1 and 3 in mouse astrocytoma: a membrane proteomics approach. *Cancer Lett.* **263:** 243–252.
57. Pedersen, P. L. 1978. Tumor mitochondria and the bioenergetics of cancer cells. *Prog. Exp. Tumor Res.* **22:** 190–274.
58. Zu, X. L., and M. Guppy. 2004. Cancer metabolism: facts, fantasy, and fiction. *Biochem. Biophys. Res. Commun.* **313:** 459–465.
59. Elstrom, R. L., D. E. Bauer, M. Buzzai, R. Karnauskas, M. H. Harris, D. R. Plas, H. Zhuang, R. M. Cinalli, A. Alavi, C. M. Rudin, et al. 2004. Akt stimulates aerobic glycolysis in cancer cells. *Cancer Res.* **64:** 3892–3899.
60. Pelicano, H., R. H. Xu, M. Du, L. Feng, R. Sasaki, J. S. Carew, Y. Hu, L. Ramdas, L. Hu, M. J. Keating, et al. 2006. Mitochondrial respiration defects in cancer cells cause activation of Akt survival pathway through a redox-mediated mechanism. *J. Cell Biol.* **175:** 913–923.
61. Kiebish, M. A., X. Han, H. Cheng, and T. N. Seyfried. 2008. Mitochondrial lipidome and electron transport chain alterations in non-metastatic and metastatic murine brain tumors. *J. Neurochem.* **104 (Suppl.):** 37–38.
62. Hartz, J. W., R. E. Morton, M. M. Waite, and H. P. Morris. 1982. Correlation of fatty acyl composition of mitochondrial and microsomal phospholipid with growth rate of rat hepatomas. *Lab. Invest.* **46:** 73–78.
63. Genova, M. L., C. Bianchi, and G. Lenaz. 2003. Structural organization of the mitochondrial respiratory chain. *Ital. J. Biochem.* **52:** 58–61.
64. Kiebish, M. A., and T. N. Seyfried. 2005. Absence of pathogenic mitochondrial DNA mutations in mouse brain tumors. *BMC Cancer.* **5:** 102.
65. Matoba, S., J. G. Kang, W. D. Patino, A. Wragg, M. Boehm, O. Gavrilova, P. J. Hurley, F. Bunz, and P. M. Hwang. 2006. p53 regulates mitochondrial respiration. *Science.* **312:** 1650–1653.
66. Limoli, C. L., E. Giedzinski, W. F. Morgan, S. G. Swarts, G. D. Jones, and W. Hyun. 2003. Persistent oxidative stress in chromosomally unstable cells. *Cancer Res.* **63:** 3107–3111.

67. Shukkur, E. A., A. Shimohata, T. Akagi, W. Yu, M. Yamaguchi, M. Murayama, D. Chui, T. Takeuchi, K. Amano, K. H. Subramhanya, et al. 2006. Mitochondrial dysfunction and tau hyperphosphorylation in Ts1Cje, a mouse model for Down syndrome. *Hum. Mol. Genet.* **15:** 2752–2762.
68. Hardy, S., W. El-Assaad, E. Przybytkowski, E. Joly, M. Prentki, and Y. Langelier. 2003. Saturated fatty acid-induced apoptosis in MDA-MB-231 breast cancer cells. A role for cardiolipin. *J. Biol. Chem.* **278:** 31861–31870.
69. Houtkooper, R. H., and F. M. Vaz. 2008. Cardiolipin, the heart of mitochondrial metabolism. *Cell. Mol. Life Sci.* **65:** 2493–2506.
70. Petrosillo, G., F. M. Ruggiero, M. Pistolese, and G. Paradies. 2004. Ca2+-induced reactive oxygen species production promotes cytochrome c release from rat liver mitochondria via mitochondrial permeability transition (MPT)-dependent and MPT-independent mechanisms: role of cardiolipin. *J. Biol. Chem.* **279:** 53103–53108.
71. McMillin, J. B., and W. Dowhan. 2002. Cardiolipin and apoptosis. *Biochim. Biophys. Acta.* **1585:** 97–107.
72. Cheng, P., and G. M. Hatch. 1995. Inhibition of cardiolipin biosynthesis in the hypoxic rat heart. *Lipids.* **30:** 513–519.
73. Han, X., J. Yang, K. Yang, Z. Zhao, D. R. Abendschein, and R. W. Gross. 2007. Alterations in myocardial cardiolipin content and composition occur at the very earliest stages of diabetes: a shotgun lipidomics study. *Biochemistry.* **46:** 6417–6428.
74. Pope, S., J. M. Land, and S. J. Heales. 2008. Oxidative stress and mitochondrial dysfunction in neurodegeneration; cardiolipin a critical target? *Biochim. Biophys. Acta.* **1777:** 794–799.
75. Yamaoka, S., R. Urade, and M. Kito. 1990. Cardiolipin molecular species in rat heart mitochondria are sensitive to essential fatty acid-deficient dietary lipids. *J. Nutr.* **120:** 415–421.
76. Kritchevsky, D. 1999. Caloric restriction and experimental carcinogenesis. *Toxicol. Sci.* **52:** 13–16.
77. Tannenbaum, A. 1959. Nutrition and cancer. *In* Physiopathology of Cancer. F. Homburger, editor. Paul B. Hober, New York. 517–562.
78. Nebeling, L. C., F. Miraldi, S. B. Shurin, and E. Lerner. 1995. Effects of a ketogenic diet on tumor metabolism and nutritional status in pediatric oncology patients: two case reports. *J. Am. Coll. Nutr.* **14:** 202–208.
79. Zhou, W., P. Mukherjee, M. A. Kiebish, W. T. Markis, J. G. Mantis, and T. N. Seyfried. 2007. The calorically restricted ketogenic diet, an effective alternative therapy for malignant brain cancer. *Nutr. Metab. (Lond).* **4:** 5.
80. Mukherjee, P., M. M. El-Abbadi, J. L. Kasperzyk, M. K. Ranes, and T. N. Seyfried. 2002. Dietary restriction reduces angiogenesis and growth in an orthotopic mouse brain tumour model. *Br. J. Cancer.* **86:** 1615–1621.
81. Mukherjee, P., L. E. Abate, and T. N. Seyfried. 2004. Antiangiogenic and proapoptotic effects of dietary restriction on experimental mouse and human brain tumors. *Clin. Cancer Res.* **10:** 5622–5629.
82. Pan, J. G., and T. W. Mak. 2007. Metabolic targeting as an anticancer strategy: dawn of a new era? *Sci. STKE.* **2007:** pe14.